Cell Reports, Volume *34*

Supplemental Information

Kmt2c mutations enhance HSC self-renewal capacity and convey a selective advantage after chemotherapy

Ran Chen, Theresa Okeyo-Owuor, Riddhi M. Patel, Emily B. Casey, Andrew S. Cluster, Wei Yang, and Jeffrey A. Magee

Supplemental figures and legends

Figure S1

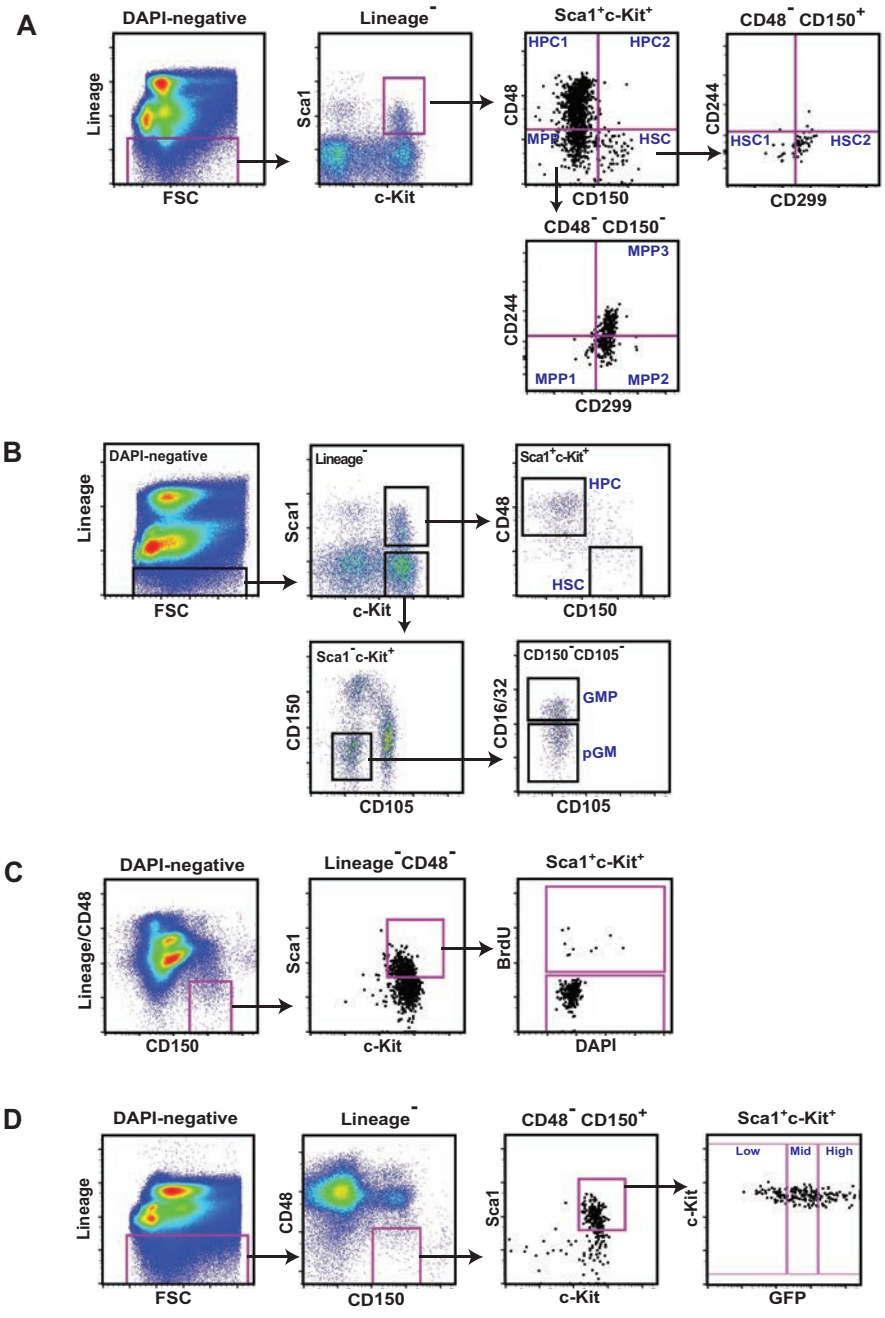

Figure S1 (related to Figures 1 and 2). Gating strategies for populations analyzed in wild type and *Kmt2c*$^{\Delta/\Delta}$ mice. (A) Representative flow plots and gating strategies for HSC, MPP and HPC subpopulations as defined by Oguro et al. (B) Representative flow plots and gating strategies for pGM and GMP populations as defined by Pronk et al. (C) Gating strategy for BrdU incorporation assays in HSCs. (D) Representative flow plots and gating strategy for H2B-GFP assays.

Figure S2

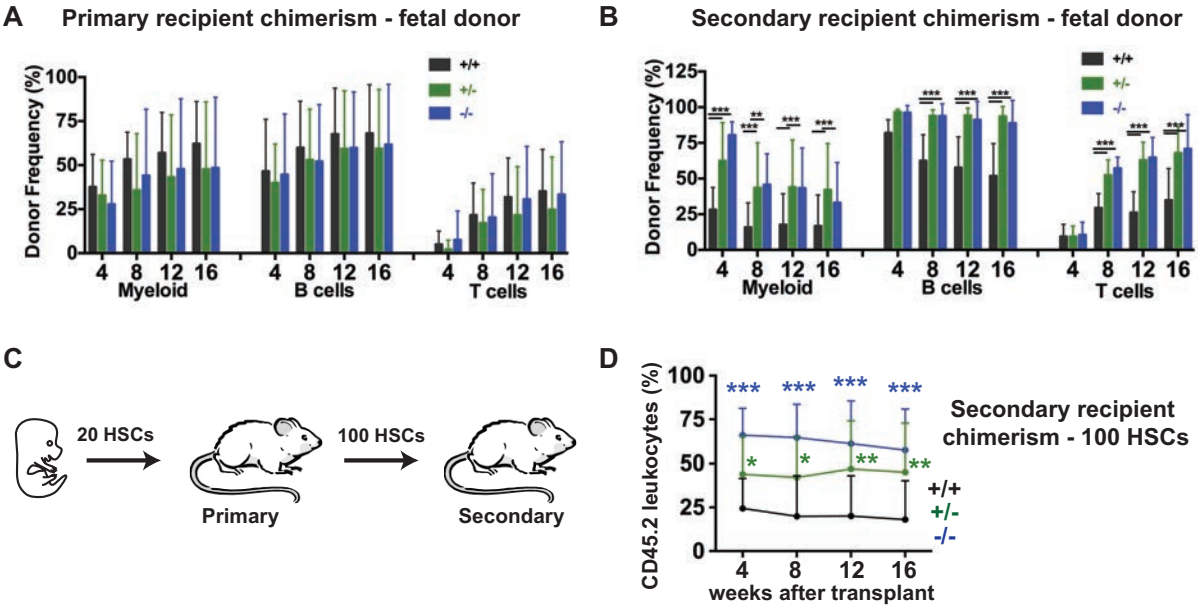

Figure S2 (related to Figure 1). Peripheral blood chimerism after fetal HSC transplants. (A, B) CD45.2 chimerism in peripheral myeloid, B- and T-cell populations in primary and secondary recipient at the indicated weeks after transplant, for the indicated genotypes. n=14-15 recipients per genotype from at least three independent donors. (C) Overview of an alternative approach to secondary transplants in which 100 sorted CD45.2^{+} HSCs (from primary recipients) were transplanted into secondary recipients with 300,000 competitor bone marrow cells. (D) CD45.2 chimerism in secondary recipients that received 100 HSCs. For all panels, error bars reflect standard deviation. *p<0.05, **p<0.01, ***p<0.001; comparisons were made by two-tailed student's t-test (single comparisons) or one-way ANOVA with Holm-Sidak post-hoc test (multiple comparisons).

Figure S3

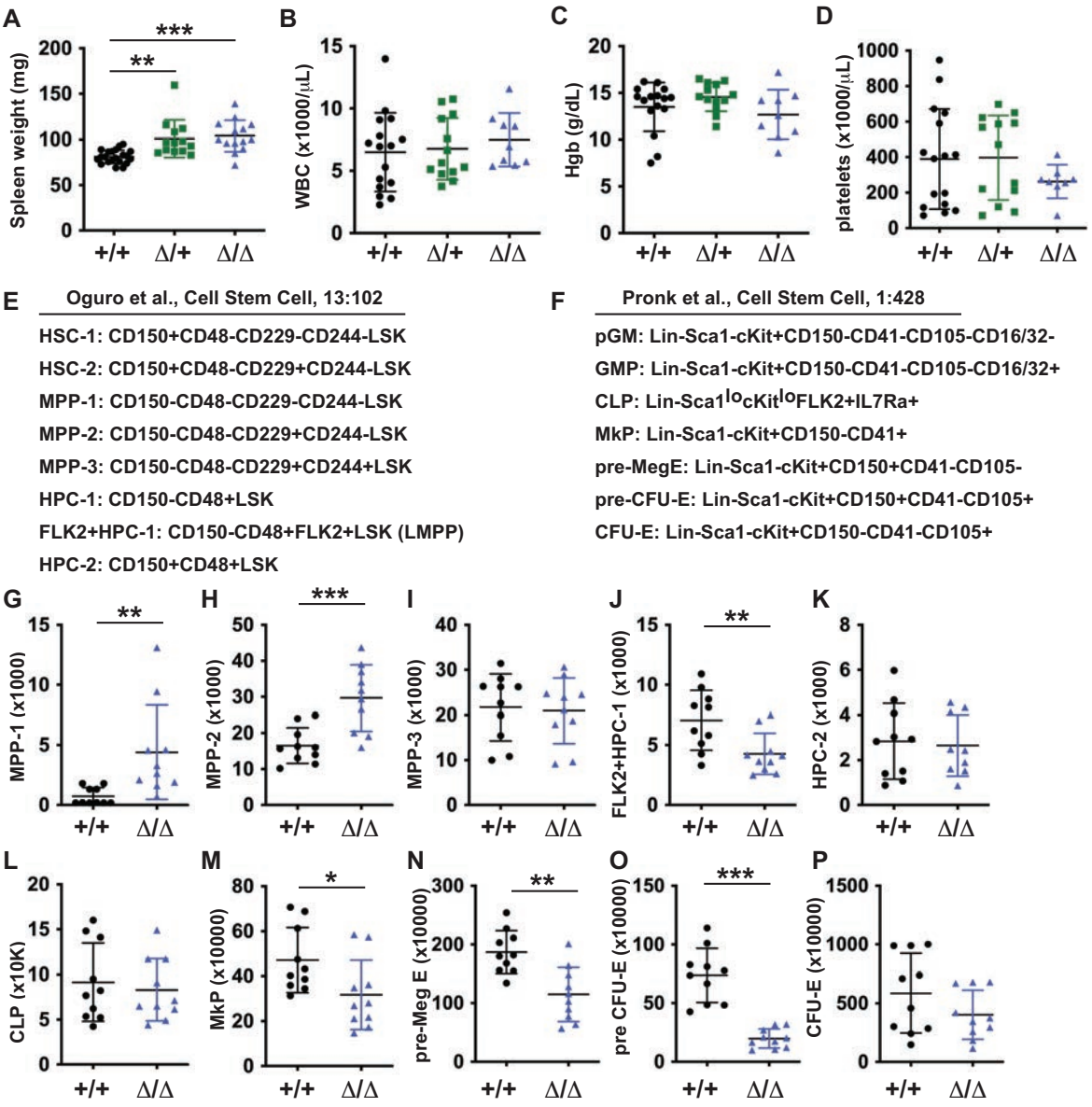

Figure S3 (related to Figure 2). Analysis of hematopoiesis after conditional *Kmt2c* deletion. (A-D) The spleen weights, white blood cell counts, hemoglobin (Hgb) and platelet counts in 8-week-old wild type, $Kmt2c^{\Delta/+}$ and $Kmt2c^{\Delta/\Delta}$ mice. (E, F) Surface marker phenotypes for HSC, MPP, HPC and myeloid progenitor sub-populations that were used in these analyses. See Figure S1 for representative gates. (G-P) Absolute numbers of the indicated HSC, MPP, HPC and myeloid progenitor sub-populations in bone marrow (two hind limbs) from wild type and $Kmt2c^{\Delta/\Delta}$ mice. n=10. Error bars reflect standard deviations. *p<0.05, **p<0.01, ***p<0.001 by two-tailed Student's t-test.

Figure S4

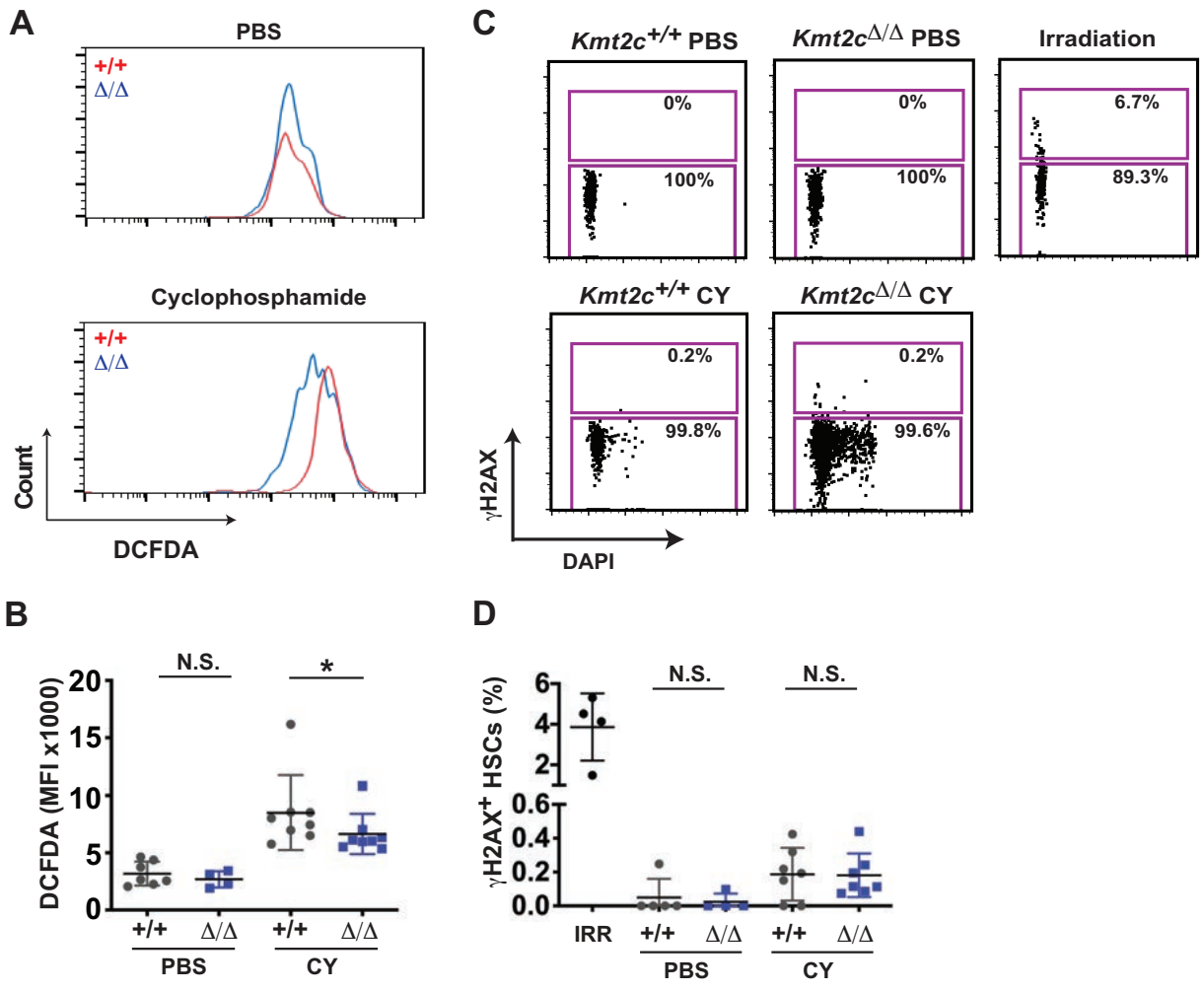

Figure S4 (related to Figure 4). *Kmt2c* deletion has limited effects on ROS levels and DNA damage. (A) Representative histograms showing DCFDA fluorescence in wild type and *Kmt2c*$^{\Delta/\Delta}$ HSCs after vehicle (PBS) or cyclophosphamide treatment. (B) Mean DCFDA fluorescence in wild type and *Kmt2c*$^{\Delta/\Delta}$ HSCs two days after vehicle (PBS) or CY treatment. n=4-8. (C) Representative flow cytometry plots and gating strategy for γH2AX detection in wild type and *Kmt2c*$^{\Delta/\Delta}$ HSCs. Irradiation (600 cGy) was used as a positive control. (D) Percent of wild type and *Kmt2c*$^{\Delta/\Delta}$ HSCs with γH2AX after irradiation (Irr), or 2 days after PBS or CY treatment. n=4-7. Error bars reflect standard deviations. *p<0.05 by two-tailed Student's t-test.

Figure S5

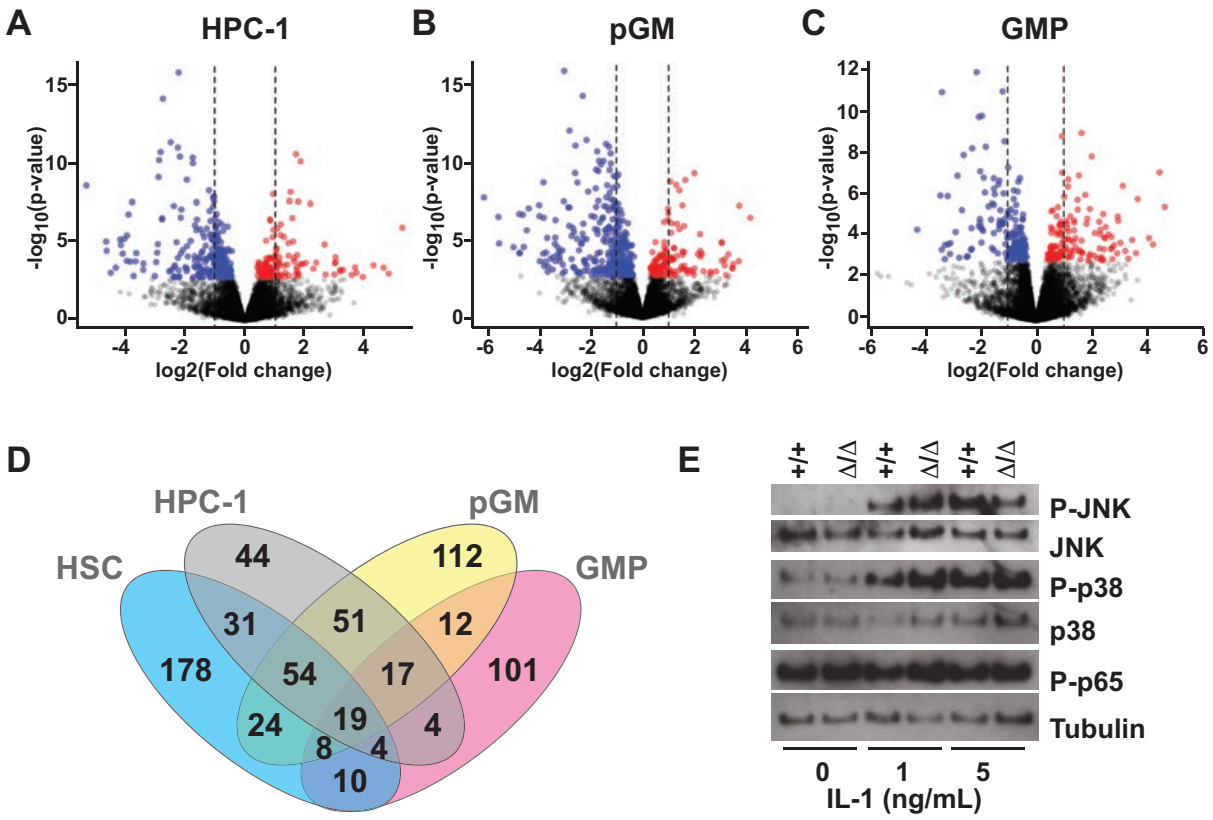

Figure S5 (related to Figure 4). *Kmt2c* deletion blunts IL-1β-driven signal transduction and gene expression changes. (A-C) Volcano plots showing gene expression changes in *Kmt2c*$^{\Delta/\Delta}$ HPC-1, pGM and GMP. n=4 per genotype. Red and blue denote significantly increased or decreased expression after *Kmt2c* deletion (FDR<0.05). n=4. (D) Venn diagram showing the degree of overlap in differentially expressed genes identified by comparing wild type to *Kmt2c*$^{\Delta/\Delta}$ HSCs, HPC-1s, pGMs and GMPs. (E) Western blots showing JNK, p38 and p65 phosphorylation in HPCs after *ex vivo* IL-1β exposure.

Figure S6

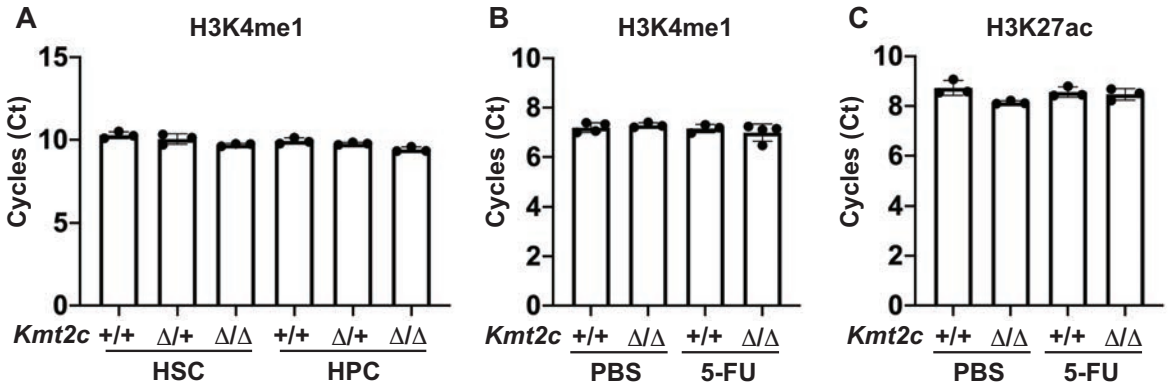

Figure S6 (related to Figures 6 and 7). *Kmt2c* deletion does not alter global H3K4me1 or H3LK27ac levels. (A, B) ChIP-qPCR with tagmented chromatin fragments from 30,000 HSCs after immunoprecipitation with H3K4me1 antibody. Cell types, treatment groups and genotypes are indicated on the x-axis. The ChIP-qPCR shows very little variation in signal among the genotypes and treatment groups, indicating that H3K4me1 levels are not globally depleted in the absence of MLL3. (C) ChIP-qPCR with tagmented chromatin fragments from 50,000 HSCs after immunoprecipitation with H3K4me1 antibody. n=3-4.

Figure S7

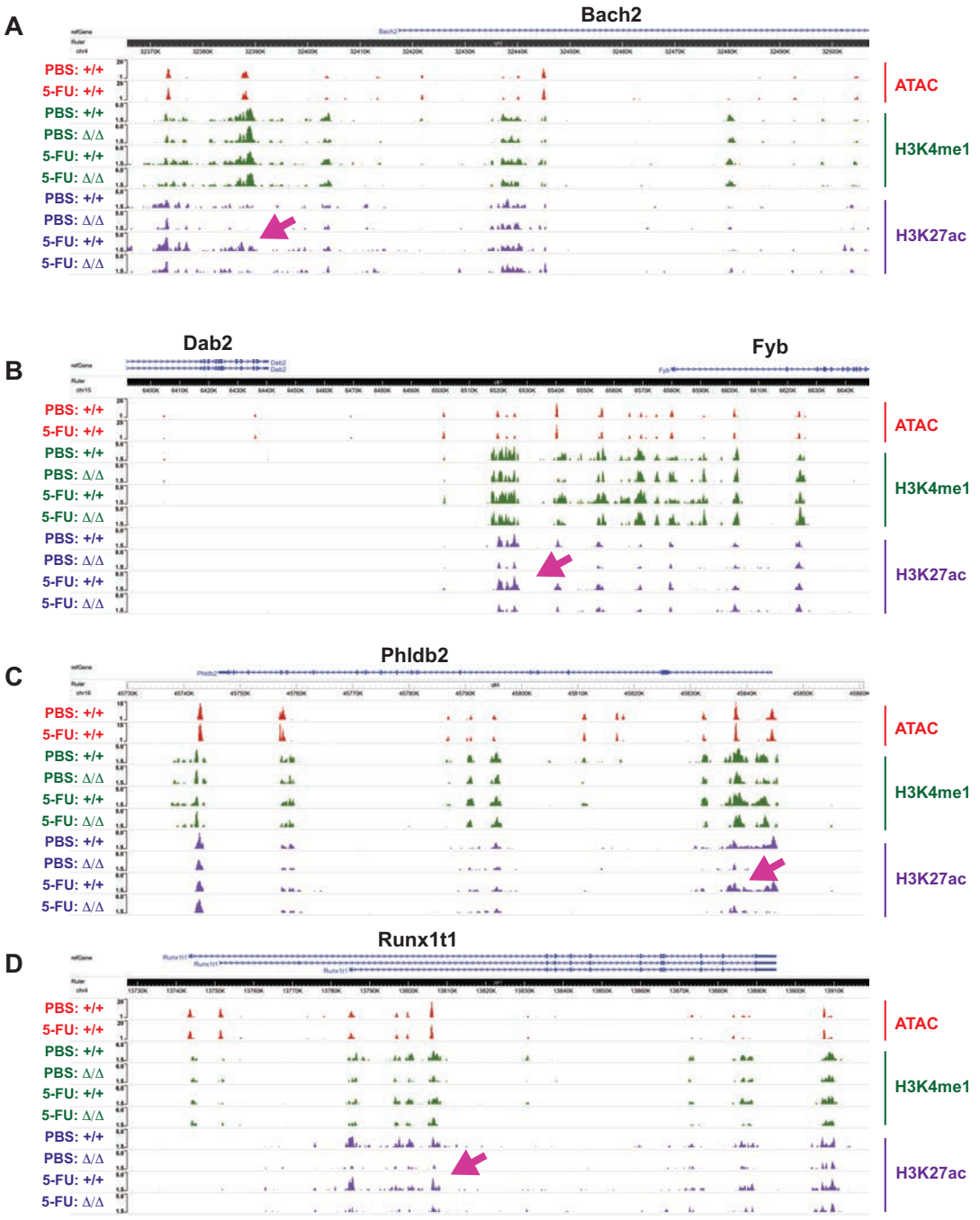

Figure S7 (related to Figure 7). MLL3 promotes enhancer activation after 5-FU treatment. (A-D) Tracks for ATAC-seq, H3K4me1 and H3K27ac levels at five MLL3 target genes – *Bach2* (A), *Dab2* and *Fyb* (B), *Phldb2* (C) and *Runx1t1* (D) – in HSCs after 3 cycles of PBS or 5-FU treatment.